Simulation of cable coupling

David W. P. Thomas

November, 2008

Abstract

This is the first report on the study of cable coupling. The work to date has involved developing models of the cable coupling phenomenon. Results are provided showing the estimate cable coupling compared with measurements. From a comparison of the braid transfer impedance models it is concluded that the Kley model seems reasonably accurate. From the measurement results provided by previous Thales reports it is apparent that stray reactances play an important role in defining the resonant points in the cable coupling. Comparable simulation results can be obtained through the application of reasonable stray reactive values. At resonance the cable coupling will only be limited by losses in the circuit. An estimate of losses is therefore required to obtain an estimate of maximum coupling. The proposed future work will therefore include the estimation of stray reactances and losses.

Contents

1 Theory of cable transfer impedance

In this section three well known models for cable transfer impedance were considered and compared for cable sheaths with a single layer weave. The models considered were the models of Vance [1], Tyni [2], and Kley [3]. Note that in the past different nomenclatures have been used for describing the models so a table is provided in the appendix comparing the nomenclature used in this report with previous work.

1.1 Sheath parameters

The basic parameters of a braided sheath as depicted in Figure 1. are:

P Picks or the number of carrier crossings per unit length

N Number of carriers

n Number of wires in each carrier

l lay length (one carrier rotation)

d wire diameter

α braid angle

h radial spindle separation.

D_o outer diameter of dielectric

D_m mean braid diameter

b hole width

The above parameters over specify the braid, so P or l are given as and the other parameter is deduced from:

$$l = \frac{N}{2P} \tag{1}$$

Braid angle α and radial spindle separation h are also calculated from (2), (3) and (4) as proposed by Katakis [4] who suggested D_m is also a function of h. The equations represent a non-linear relationship so a solution is found through a Newton-Raphson iteration of the equations.

$$\tan\alpha = \frac{2\pi D_m P}{N} \tag{2}$$

$$\left[\frac{2\pi}{N}\cos\alpha\right] h^2 + \left[(1-n)d + \frac{2\pi}{N}(D_o + 2d)\cos\alpha\right] h - 2d^2 = 0 \tag{3}$$

$$D_m = D_o + 2d + h \tag{4}$$

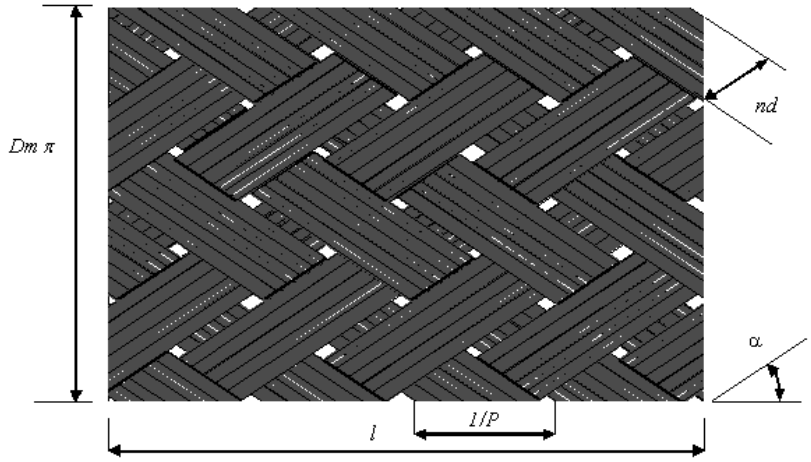

Figure 1: Detail of the sheath showing defined parameters

Once h and *alpha* are found then

$$b = \frac{2\pi D_m}{N}\cos\alpha - nd \tag{5}$$

These then are all the parameters necessary to define the shield for the calculation of the transfer impedance. A typical set of cable parameters can be found in [5].

1.2 Vance model

The Vance model [1] is one of the earliest and simplest models which takes into account skin depth and braid inductance. The DC resistance of the braid is given by

$$R_c = \frac{4}{\pi d^2 n N \sigma \cos\alpha} \tag{6}$$

Then allowing for the skin depth effect the screen impedance can be found from [7]

$$Z_d = R_c \frac{(1+j)d/\delta}{\sinh((1+j)d/\delta)} \tag{7}$$

where the skin depth $\delta$is given by

$$\delta = \frac{1}{(\pi f \mu_0 \sigma)^{1/2}} \tag{8}$$

Additionally to the screen impedance is a braid inductance M which is given by

$$M = \frac{\pi \mu_0}{6N}(1-\chi)^{3/2}\frac{e^2}{E(e)-(1-e^2)K(e)} \tag{9}$$
$$e = (1-\tan^2\alpha)^{1/2} \quad \text{if} \quad \alpha < 45^o$$

or

$$M = \frac{\pi \mu_0}{6N}(1-\chi)^{3/2}\frac{\frac{e^2}{\sqrt{1-e^2}}}{E(e)-(1-e^2)K(e)} \tag{10}$$
$$e = (1-\cot^2\alpha)^{1/2} \quad \text{if} \quad \alpha > 45^o$$

where $K(e)$ and $E(e)$ are complete elliptic integrals of the first and second kind, respectively, defined by

$$K(e) = \int_0^{\pi/2} \frac{d\varphi}{(1-e^2\sin^2\varphi)^{1/2}} \tag{11}$$

$$E(e) = \int_0^{\pi/2} (1-e^2\sin^2\varphi)^{1/2} d\varphi \tag{12}$$

F is fill factor of braid given by

$$F = \frac{nNd}{2\pi D_m \cos\alpha} \tag{13}$$

F_0 is the minimal filling factor given by

$$F_0 = F\cos\alpha \tag{14}$$

and the optical coverage χ is given by

$$\chi = 2F - F^2 \tag{15}$$

The total transfer impedance is then given by

$$Z_T(f) = Z_d(f) + 1j\omega M \tag{16}$$

1.3 Tyni model

In the Tyni model [2] the transfer impedance is found from the braid inductance L_b and the leakage or gap inductance L_h due to the gaps in the screen. This model was studied extensively in [8] and found to be reasonably accurate.

$$L_b = \frac{\mu_0 h}{4\pi D_m}(1 - tan^2\alpha) \tag{17}$$

$$L_h = \frac{\mu_0 2N}{\pi cos\alpha}\left(\frac{b}{\pi D_m}\right)^2 exp\left(\frac{-\pi d}{b} - 2\right) \tag{18}$$

The transfer impedance Z_t is then given by

$$Z_t = Z_d + j\omega(L_h - L_b) \tag{19}$$

where Z_d is the braid impedance allowing for skin depth given by 7

1.4 Kley model

The Kley model [3]is the best and most rigorously developed of the three models and the Thales report 3.3 RCTR study [7]suggests that this is probably the more accurate.

In the Kley model there are inductances; M_l due to the apertures allowing for the curvature of the screen, M_g mutual inductance between carriers in the braid and and an inductive term due L_s to the tangential components of the electromagnetic field.

These inductances are given by the following equations

$$M_l = 0.875M\exp(-\tau_h) \tag{20}$$

$$M_g = \frac{-0.11}{Nn}\mu_0\cos(2K_1\alpha) \tag{21}$$

$$L_s = \frac{1}{\omega\pi\sigma\delta}[D_l^{-1} + D_g^{-1}] \tag{22}$$

where M is given by 10 and

$$\tau_h = 9.6F\sqrt[3]{\chi^2 d/D_m} \tag{23}$$

$$K_1 = \frac{\pi}{4}\left[\frac{2}{3}F_0 + \frac{\pi}{10}\right] \tag{24}$$

$$D_l^{-1} = \frac{10\pi F_0^2\cos\alpha}{D_m}[1 - F]\exp(-\tau_E) \tag{25}$$

$$D_g^{-1} = \frac{-3.3}{2\pi F_0 D_m}\cos(2K_2\alpha) \tag{26}$$

$$\tau_F = 12F\sqrt[3]{\chi^2 d/D_m} \tag{27}$$

$$K_2 = \frac{\pi}{4}\left[\frac{2}{3}F_0 + \frac{3}{8}\right]^{-1} \tag{28}$$

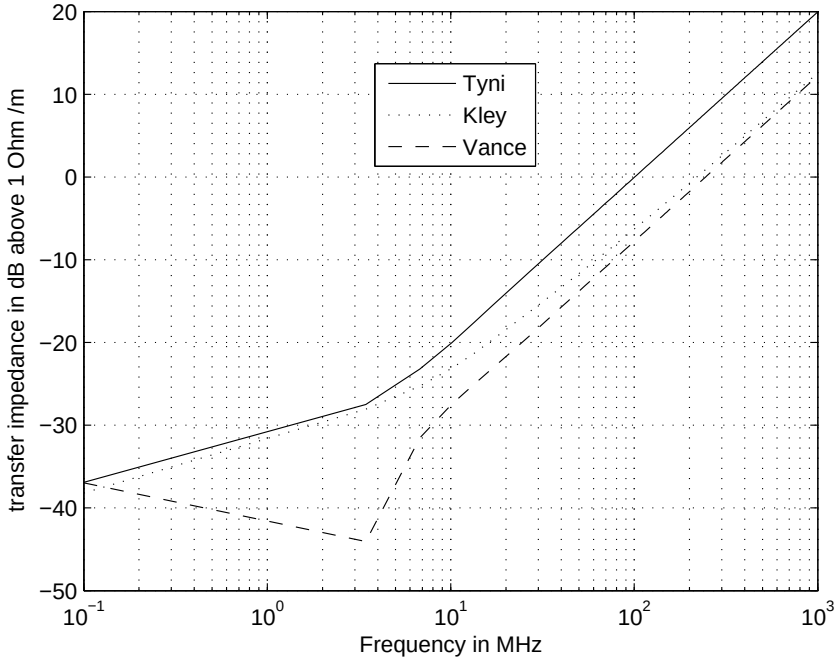

Figure 2: Predicted transfer impedance using parameters (RG58-Man.)

1.5 Comparison of the transfer impedance models

The predicted transfer impedance as given by the Vance, Tyne and Klay models for the common cable type RG58 with the parameters as supplied by the manufacturers (RG58-Man in appendix) are given in Figure 2 . There is a significant difference between the models but they are comparable to the typical results shown in Figure 3 [6] and a previous report [7] found that the Kley model gave the best results. Benson et al. [8] also reported that the Tyni model tended to over estimate the cable transfer impedance. Figure 4 shows the predicted transfer impedance using other RG58 parameters as given in [5] and by comparing this to Figure 2 this indicates by how much the transfer impedance may vary between manufacturers. In this report the Kley model and the parameters (RG58-Man) given in the appendix will be predominantly used.

Figures 5 - 7 show the predicted transfer impedances and their variance after applying a reasonable estimate of the manufacturers tolerances using the (RG58-Man) parameters. The assumed manufacturers tolerances are given in Table 1 are as used by Benson et al. [8] and the statistical distribution was assumed to be constant. Note that α and b are dependent variables.

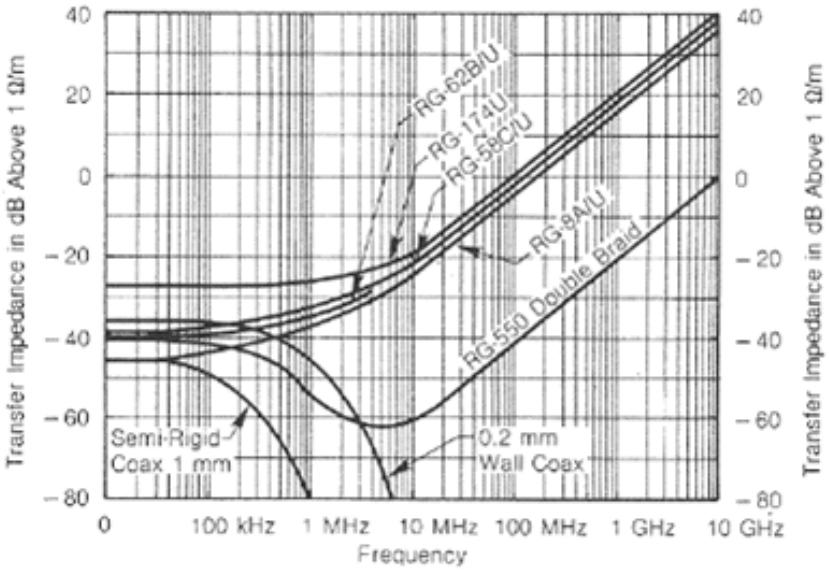

Figure 3: Typical transfer impedances of different cables [6]

Table 1. Variance in braid parameters

σ_{D0}	σ_d	σ_l
0.13 mm	0.003 mm	1.979 mm

The standard deviation, skew and kurtosis of the distribution of the predicted transfer impedances assuming a constant distribution for the tolerances are given in Figures 8 to 10. There is only a small skew and kurtosis so the variation in transfer impedance can be considered to be a normal distribution.

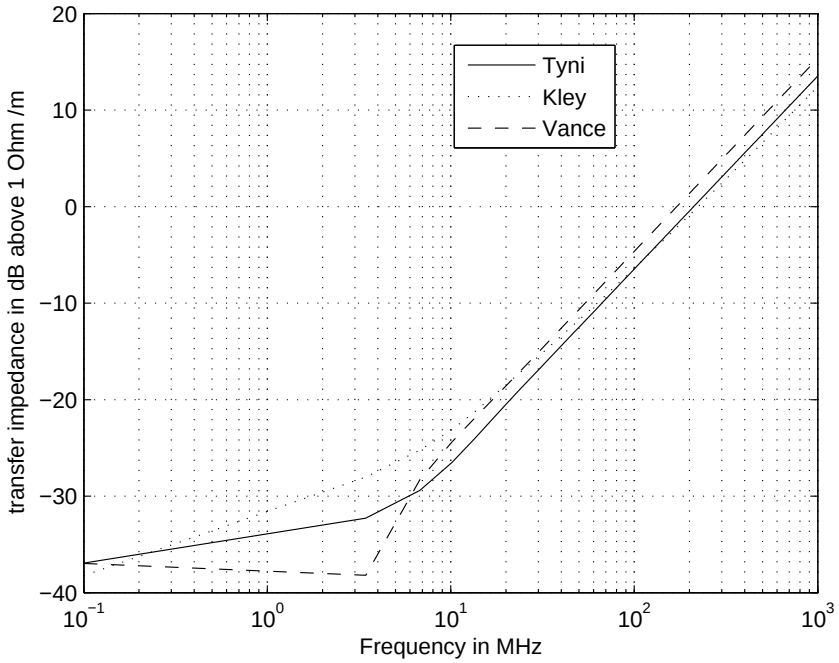

Figure 4: Predicted transfer impedance using parameters (RG58) [6]

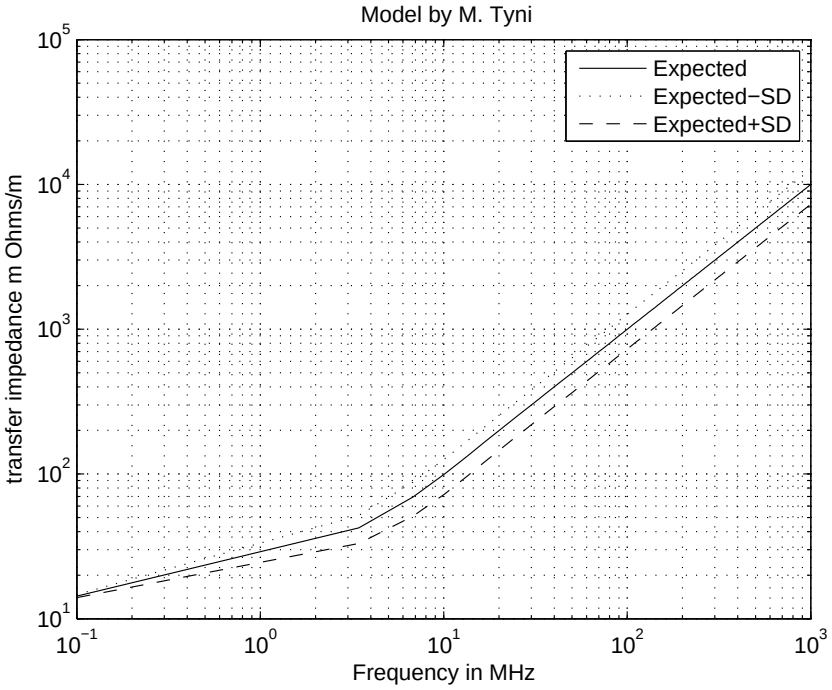

Figure 5: Predicted transfer impedance and its variance using the Tyni model [2] and manufacturing tolerances for (RG58-Man.)

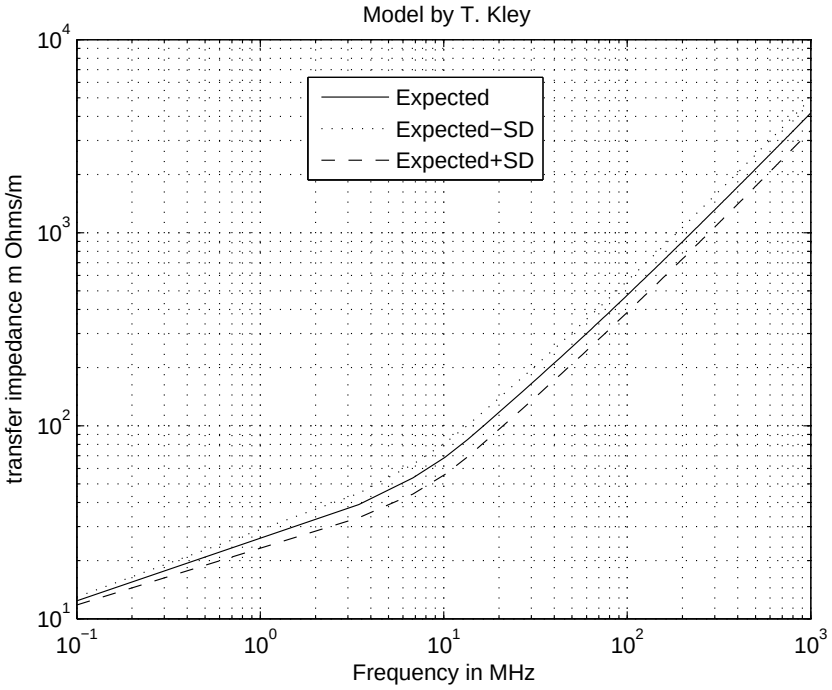

Figure 6: Predicted transfer impedance and its variance using the Kley model [3] and manufacturing tolerances for (RG58-Man.)

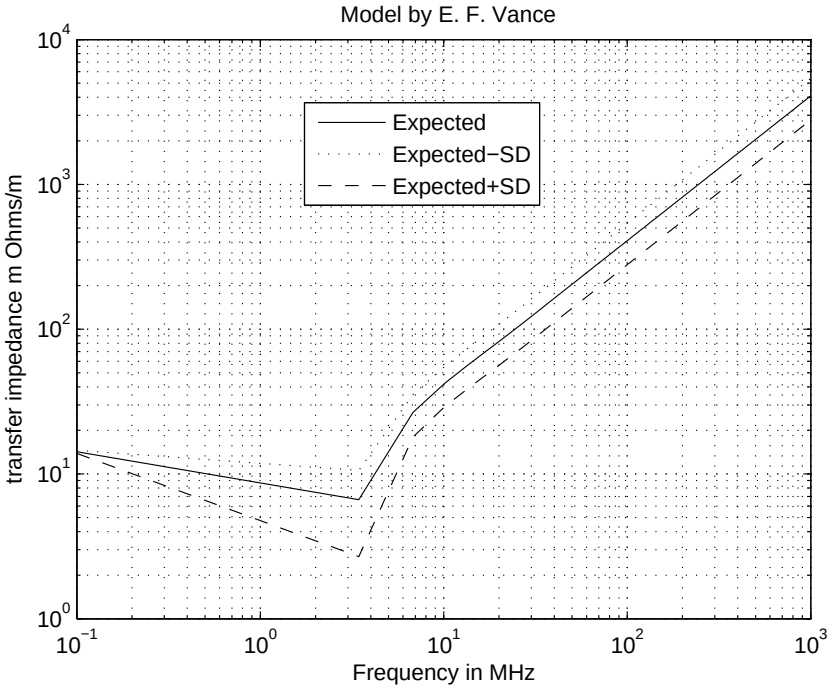

Figure 7: Predicted transfer impedance and its variance using the Vance model [1] and manufacturing tolerances for (RG58-Man.)

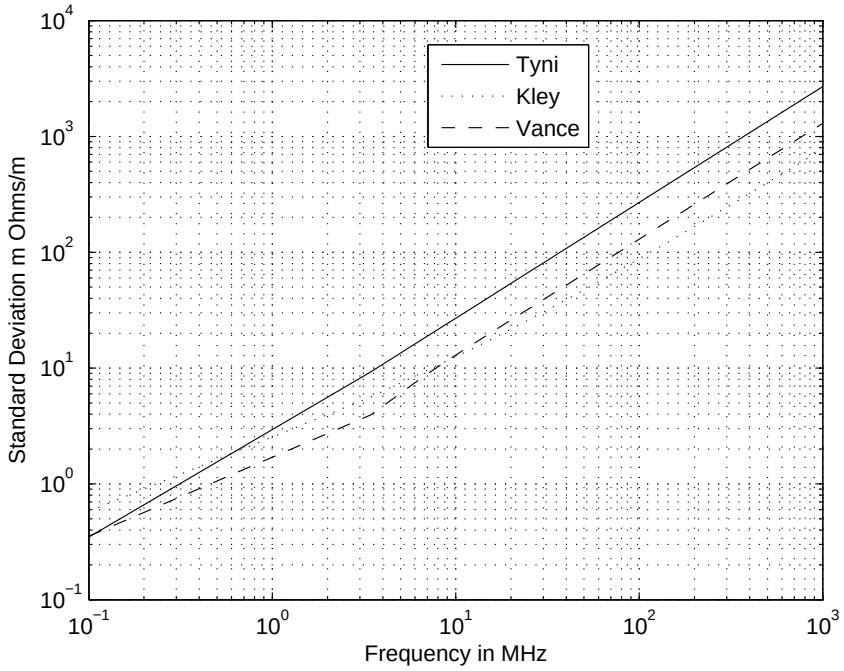

Figure 8: Predicted standard deviation in the transfer impedance using manufacturing tolerances for (RG58-Man.)

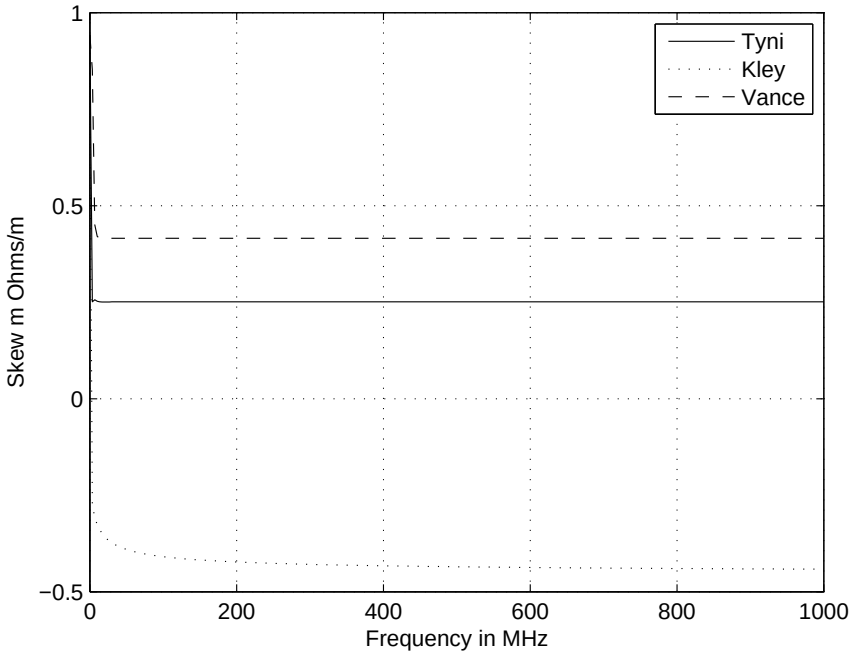

Figure 9: Predicted skew in the statistical distribution in the transfer impedance using manufacturing tolerances for (RG58-Man.)

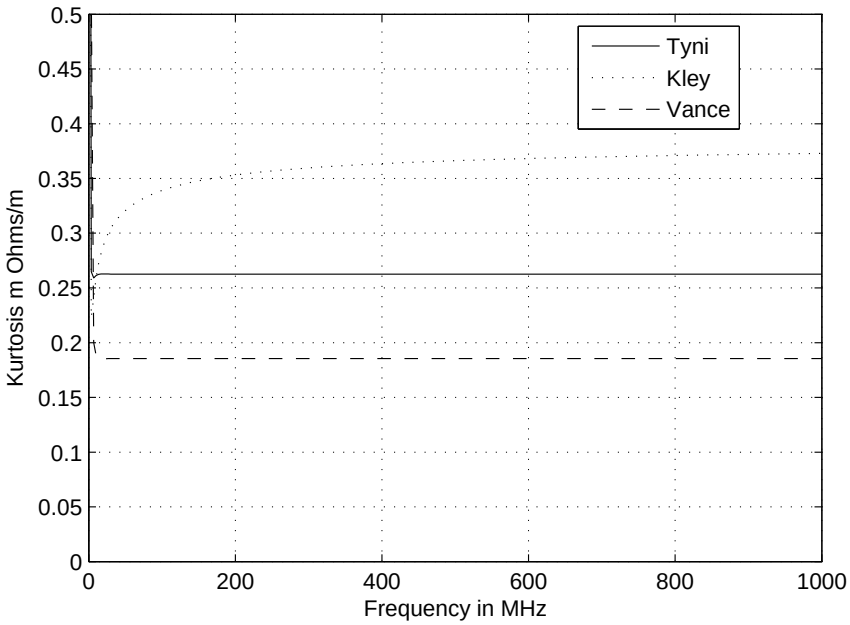

Figure 10: Predicted kurtosis in the statistical distribution in the transfer impedance using manufacturing tolerances for (RG58-Man.)

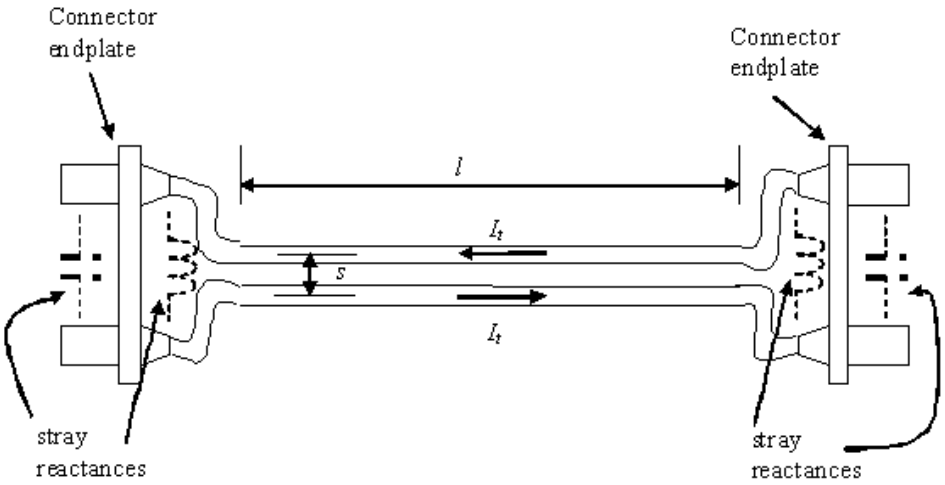

Figure 11: A typical cable layout of two parallel cables showing points were significant stray reactances can affect coupling

2 Theory of cable coupling via the braid transfer impedance

In this work the cable coupling due to transfer impedance alone is considered. The effect of transfer admittance has not been included as for non optimized cable sheaths it should only have a small effect [9, 10]. Coupling due to the effect of a transfer impedance will occur between cables when they are laid roughly in parallel along a common path. A typical cabling arrangement is shown in Figure 11 where the cables have approximately a constant separation along a length l, for instance due to being laid in cable trunking, but the cables normally diverge near their connection points. The nature of the terminations strongly effects the degree of cable coupling at high frequencies due to the stray reactances they introduce. If the cables are connected to a common connector endplate (or common cabinet) then the stray reactance will be inductive due to the introduction of an extra loop area, but if the cables are connected to electrically isolated units then the stray reactance will be mostly capacitive. These stray reactances at the terminations can only be estimated due to the geometric complexity of the terminations and the lack of known details. The terminations are therefore the main limit to the accuracy to which the cable coupling can be predicted.

The equivalent circuit for the coupling path created by the cable sheath transfer impedance is shown in Figure 12. The currents I_s along the source

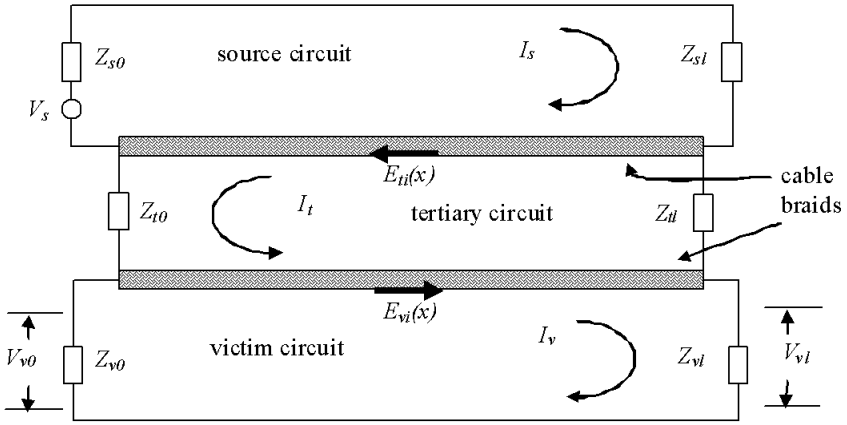

Figure 12: Equivalent circuit for cable coupling between two shielded cables via the shield transfer impedance

cable creates a voltage gradient $E_{it}(x)$ along the outer sheath given by

$$E_{it}(x) = Z_{ts} I_s(x) \tag{29}$$

where Z_{ts} is the shield transfer impedance of the source cable and x is the distance along the cable sheath. The voltage gradient on the source cable will then induce a current on the outer sheath of the victim cable. This induced current circulates around a circuit composed of the outer sheaths of the two parallel cables and termed the tertiary circuit. For low frequencies ($\lambda >>$ the length of the cables) the sheath voltage gradient is independent of x. The equivalent circuit for low frequency coupling to a transmission line is as given in Figure 13. the induced current in the tertiary circuit I_t is then given by

$$I_t = \frac{E_{it} l}{j\omega L_{tl} l + Z_{t0} + Z_{tl}} = \frac{Z_{ts} I_s l}{j\omega L_{tl} l + Z_{t0} + Z_{tl}} \tag{30}$$

where $\omega = 2\pi f$ is the angular frequency , L_t is the inductance per unit length of the tertiary cable pair, Z_{t0} and Z_{tl} are the termination impedances at each end of the tertiary circuit (i.e. they represent the termination stray reactances in parallel with half the total transmission line capacitance) and l is the length over which the cables are approximately parallel. For cables laid closely together $\omega L_{tl} l$ may be comparable to Z_{t0} and Z_{tl} and hence the difficulty in estimating the cable coupling.

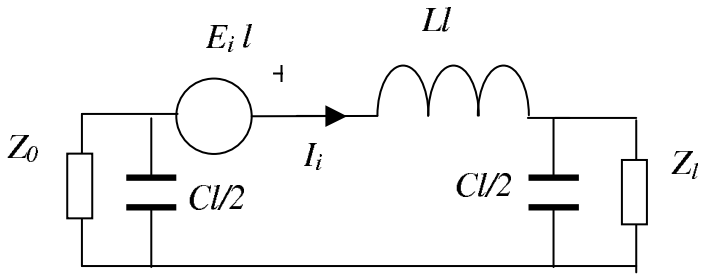

Figure 13: Equivalent circuit for low frequency cable coupling

The induced tertiary current will in turn induce a current I_v in the victim cable due to the induced voltage gradient $E_{vi}(x)$ caused by the victims sheath transfer impedance Z_{tv}, as shown in Figure 12. The induced victim current will then creates a voltage across the terminations of the victim cable which is the usual measurable form of the cable coupling. For example the voltage across terminal 0 of the victim V_{v0} will be given by

$$V_{v0} = \frac{Z_{tv} I_t l Z_{v0}}{Z_{v0} + Z_{vl}} = \frac{Z_{tv} Z_{ts} I_s l^2 Z_{v0}}{(Z_{v0} + Z_{vl})(j\omega L_{tl} l + Z_{t0} + Z_{tl})} \tag{31}$$

where Z_{v0} and Z_{vl} are the termination impedances of the victim circuit.

The cable coupling is then quantified by the ratio of the received victim voltage to the source voltage. The coupling C in dB is then defined as

$$C = 20 \log_{10} \left(\frac{V_{v0}}{V_s} \right) \tag{32}$$

The current in the tertiary circuit is often called the common mode current but in fact it has the form of a differential mode as the victim and source currents are of opposite sign. The presence of another cable or a ground plane will enable other current paths to form and reduce the coupling between two cables. In the case of an additional ground plane the induced tertiary circuit current would have two modes of the form of a differential and common mode. The general equivalent coupling circuit for two cables above a ground plane can be represented by the circuit given in Figure 14. The differential and common

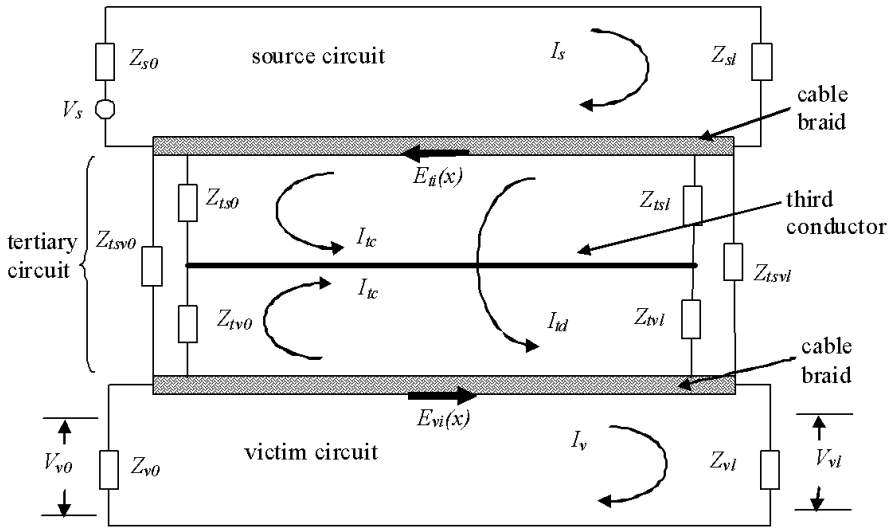

Figure 14: Equivalent circuit for cable coupling between two shielded cables via shield transfer impedance in the presence of a third conductor (ground plane of third cable shield)

mode currents (I_{td} and I_{tc}) on the cable sheaths are related to the total sheath currents on the source cable and victim cable (I_{ts} and I_{tv} respectively) by

$$\begin{bmatrix} I_{ts} \\ I_{tv} \end{bmatrix} = \begin{bmatrix} -1 & 1 \\ 1 & 1 \end{bmatrix} \begin{bmatrix} I_{td} \\ I_{tc} \end{bmatrix} \tag{33}$$

or

$$[I_{tsv}] = [S][I_{tcd}] \tag{34}$$

where $[I_{tsv}]$ is the vector of cable sheath currents, $[I_{tcd}]$ is the vector of common mode and differential mode currents and $[S]$ is the modal transformation matrix. For low frequencies ($\lambda >>$ the length of the cables) the induced common mode and differential mode currents on the tertiary circuit cable sheaths are then related to the source sheath voltage ($E_{ti}l$) by

$$\begin{bmatrix} E_{ti}l \\ 0 \end{bmatrix} = \left(j\omega l \begin{bmatrix} L_{ts} & L_{tm} \\ L_{tm} & L_{tv} \end{bmatrix} + [Z_{t0}] + [Z_{tl}] \right) \begin{bmatrix} I_{ts} \\ I_{tv} \end{bmatrix} \tag{35}$$

where L_{ts} and L_{tv} are the self inductance of the source and victim shields respectively, L_{tm} is the mutual inductance between the source and victim cable shields, $[Z_{t0}]$ and $[Z_{tl}]$ are the impedance matrices of the tertiary circuit terminations as depicted in figure 14 and these then have the form

$$[Z_{tX}] = \begin{bmatrix} \frac{Z_{tsx}(Z_{tvx}+Z_{tsvx})}{Z_{tsvx}+Z_{tsx}+Z_{tvx}} & \frac{Z_{tsx}Z_{tvx}}{Z_{tsvx}+Z_{tsx}+Z_{tvx}} \\ \frac{Z_{tsx}Z_{tvx}}{Z_{tsvx}+Z_{tsx}+Z_{tvx}} & \frac{Z_{tvx}(Z_{tsx}+Z_{tsvx})}{Z_{tsvx}+Z_{tsx}+Z_{tvx}} \end{bmatrix} \tag{36}$$

where $X = 0$ or l

Equation (35) is then solved for the victim current I_{tv} which can then be substituted for I_t in (31) to find the induced voltage across the victim termination/connector.

For higher frequencies the voltage per unit length along the source cable sheath will have a significant variation along the cable length due to propagation effects and these need to be taken into account. The propagation effects lead to resonances in the tertiary circuit and a significant increase in cable coupling.

2.1 High frequency cable coupling

For high frequencies the cable currents are no longer uniform and the propagation effects have to be considered. For a general source cable with supply impedance Z_{s0} and load impedance Z_{sl} the the input current $I_s(0)$ at the supply connector is related to the supply voltage V_s by

$$I_s(0) = \frac{V_s}{Z_{s0} + Z_c \left[\frac{Z_{sl} + Z_c \tanh \gamma_s l}{Z_c + Z_{sl} \tanh \gamma_s l}\right]} \tag{37}$$

where Z_c is the characteristic impedance of the source cable (i.e. typically 50 Ω) and γ_s is the propagation constant of the cable (i.e. $\gamma_s \approx j\omega/u$ where u is typically 2c/3). The current can also be defined in terms of forward and backward propagating waves such that

$$I_s(0) = I_s^+ + I_s^- = I_s^+ + \rho_{is} I_s^+ \tag{38}$$

where

$$\rho_{is} = \left[\frac{Z_c - Z_{sl}}{Z_{sl} + Z_c}\right] e^{-2\gamma_s l} \tag{39}$$

Thus (37) and (38) can be combined to give

$$I^+ = \frac{[Z_c + Z_{sl}] e^{\gamma_s l} V_s}{2[Z_{sl}(Z_c \cosh \gamma_s l + Z_{sl} \sinh \gamma_s l) + Z_c(Z_{sl} \cosh \gamma_s l + Z_c \sinh \gamma_s l)]} \tag{40}$$

The current along the source cable is then given by

$$I_s(x) = [e^{-\gamma_s x} + \rho_{is} e^{\gamma_s x}] I^+ \tag{41}$$

where x is the distance along the cable from the supply point. The voltage gradient along the shield of the source cable is then also a function of x as given by

$$E_{ti}(x) = Z_{ts} I_s(x) \tag{42}$$

The cable sheath tertiary circuit and the victim cable will be equivalent to transmission lines with a distributed series voltage source of the form as shown in the line section given in Figure 15. The differential equations describing the

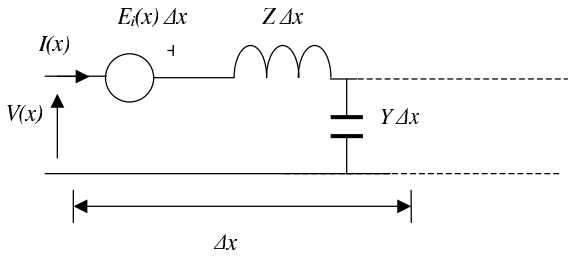

Figure 15: Equivalent circuit a section Δx of a transmission line with a distributed series voltage source.

induced voltagesV_i and currents I_i on transmission lines with a distributed series voltage source $E_i(x)$ are given by Vance [5].

$$\frac{\partial V_i}{\partial x} = E_i(x) - I_i Z \tag{43}$$

$$\frac{\partial I_i}{\partial x} = -YV_i \tag{44}$$

where Z and Y are the transmission line series impedance and shunt admittance respectively. Equations (43) and (44) can be differentiated and combined to give

$$\frac{\partial^2 V_i}{\partial x^2} - \gamma^2 V_i = \frac{\partial E_i(x)}{\partial x} \tag{45}$$

$$\frac{\partial^2 I_i}{\partial x^2} - \gamma^2 I_i = -YE_i(x) \tag{46}$$

Equation (46) has a general solution of the form [5] :

$$I_i(x) = [K_1 + P(x)]e^{-\gamma x} + [K_2 + Q(x)]e^{\gamma x} \tag{47}$$

where

$$P(x) = \frac{1}{2Z_c}\int_0^x e^{\gamma u} E_i(u)du \tag{48}$$

$$Q(x) = \frac{1}{2Z_c}\int_x^l e^{-\gamma u} E_i(u)du \tag{49}$$

and K_1 and K_2 are set to satisfy the boundary conditions at $x = 0$ and $x = l$ which gives

$$K_1 = \rho_1 \left[\frac{\rho_2 P(l)e^{-\gamma l} - Q(0)e^{\gamma l}}{e^{\gamma l} - \rho_1\rho_2 e^{-\gamma l}}\right] \tag{50}$$

$$K_2 = \rho_2 e^{-\gamma l}\left[\frac{\rho_1 Q(0) - P(l)}{e^{\gamma l} - \rho_1\rho_2 e^{-\gamma l}}\right] \tag{51}$$

where $Z_c = \sqrt{Z/Y}$, $\gamma = \sqrt{ZY}$ and

$$\rho_1 = \frac{Z_0 - Z_c}{Z_0 + Z_c} \tag{52}$$

$$\rho_2 = \frac{Z_l - Z_c}{Z_l + Z_c} \tag{53}$$

Equation (47) is therefore used to first find the currents induced on the tertiary cable sheath circuit and then it is also applied to the victim cable using the deduced tertiary current profile to deduce the induced victim current and the voltage induced across the victim terminals using.

$$V_{v0} = Z_{v0} I_{vi}(0) \tag{54}$$

$$V_{vl} = Z_{vl} I_{vi}(l) \tag{55}$$

For multiple cables or cables in the presence of a ground plane the currents induced on each of the cable sheaths will be different and the governing equations will comprise of N simultaneous equations where $N =$ the number of cables in the presence of a ground plane or $N + 1$ is the total number of cables when a ground plane is not present. The governing equations are then

$$\left[\frac{\partial^2 V_i}{\partial x^2}\right] - [Z][Y][V_i] = \left[\frac{\partial E_s(x)}{\partial x}\right] \tag{56}$$

$$\left[\frac{\partial^2 I_i}{\partial x^2}\right] - [Y][Z]\,[I_i] = -\,[Y]\,[E_i(x)] \tag{57}$$

where [X] represents now a vector of the N components of X. Equations (56) and (57) therefore represent N simultaneous equations. However if we transform the components into model components using

$$[X_m] = [S]^{-1}[X] \tag{58}$$

where $[S]$ is the transformation matrix comprising of the eigen vectors of $[Y][Z]$ then (57) has the form of N independent equations

$$\left[\frac{\partial^2 I_{im}}{\partial x^2}\right] - [\gamma_m]^2\,[I_i] = -[S]^{-1}\,[Y]\,[S]\,[E_{im}(x)] \tag{59}$$

where $[\gamma_m]^2$ is a diagonal matrix of the eigen values of $[Y][Z]$ and the general solution is of the form:

$$[I_i(x)] = [[K_1] + [P(x)]][e^{-\gamma x}] + [[K_2] + [Q(x)]][e^{\gamma_m x}] \tag{60}$$

where

$$[K_1] = [\rho_1]([e^{\gamma l}] - [\rho_1][\rho_2][e^{-\gamma l}])^{-1}([\rho_2][P(l)][e^{-\gamma l}] - [Q(0)][e^{\gamma l}]) \tag{61}$$

$$[K_2] = [\rho_2][e^{-\gamma l}]([e^{\gamma l}] - [\rho_1][\rho_2][e^{-\gamma l}])^{-1}([\rho_1][Q(0)] - [P(l)]) \tag{62}$$

where

$$[\rho_1] = ([Z_0] + [Z_c])^{-1}([Z_0] - [Z_c]) \quad \rho_2 = ([Z_l] + [Z_c])^{-1}([Z_l] - [Z_c]) \tag{63}$$

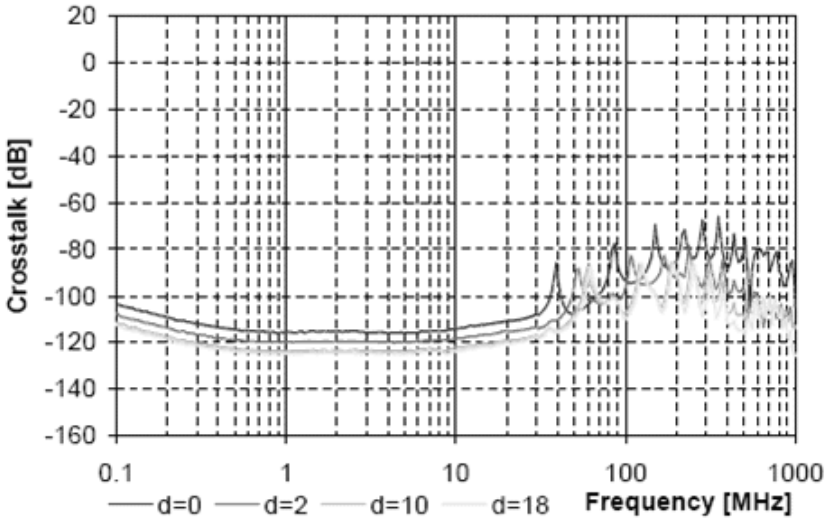

Figure 16: Measurement of Crosstalk in two RG58 coax cables (l= 2m, and common connector plates) [11].

3 Comparison of theoretical predictions with measurements

For this initial study to results were used from the internship report by Leon Korteweg [11]. The two results considered were for measurements of crosstalk between two RG58 cables. In the first example the cables were 2m long and they terminated into the same connector plate. In the second example the cables were of different lengths and the remote termination of the cables were not connected to the same connector plate (termed a floating set up in [11]). The results from these measurements are given in Figures 16 and 17 (which are Figures 4-49 and 4-46 in the report). What is immediately apparent in the results provided is that the first resonance does not correspond to the expected half wavelength frequency (75MHz for a cable length of 2m) therefore stray reactances in the tertiary circuit must be important (the cables circuits have matched loads so do not resonate).

The theoretical prediction for the coupling between the 2m length cables with the common connector plates and using the low frequency model is given in Figure 18. Notice that this model can not predict the point at which there is resonance in the tertiary circuit which leads to an increased cable coupling.

Figure 19 shows the simulation results for the more complete high frequency model and giving the tertiary terminations as a stray inductance of 1/3 μH to represent the loop inductance at the connector plate. The results in Figure 19

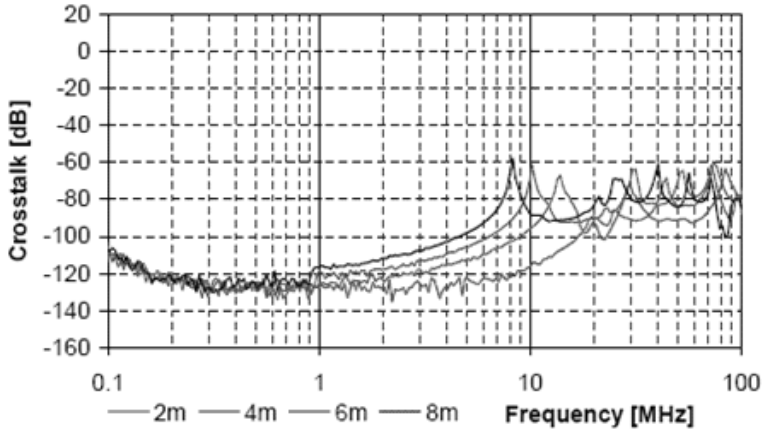

Figure 17: Measurement of Crosstalk at different cable lengths (2× RG58, d=5cm, floating cables) [11].

compare well with the measurements. The resonant frequencies are the same, but this depends on the approximated tertiary terminal impedance. The overall predicted coupling is about 10 dBs lower than the measurements. This may be due to the model of the cable transfer impedance. Figure 20 Shows the predicted cable crosstalk using the upper bound of the expected transfer impedance given the manufacturing tolerances of the cable braid. This result agrees better with the measurement results and it can also be noticed that errors in the predicted transfer impedance does not affect the predicted resonant frequencies. The other possibility is that the Klay model [3]is not sufficiently accurate. Simulations using the Vance [1] and Tyni [2] transfer impedance models are given in Figures 21 and 22 respectively. It appears that the Tyni and Vance models do not reproduce the observed cable cross coupling as well as the Klay model.

The simulation of the "floating" cables using a tertiary circuit termination impedance of 10 pF, to represent stray capacitance, is shown in Figure 23. The model appears to predict the resonances reasonably well. Below but the overall the coupling appears to be about 20 dBs too low and this may possibly due to manufacturing tolerances of the braid or incorrect braid data. Below 1 MHz the observed cable coupling is a lot greater than the predicted coupling but this may be due to the noise floor of the measurements.

4 Conclusions and suggestions for future work

From the results of the work so far it appears that a reasonable estimate of cable coupling can be made but the degree of cable coupling is significantly effected by

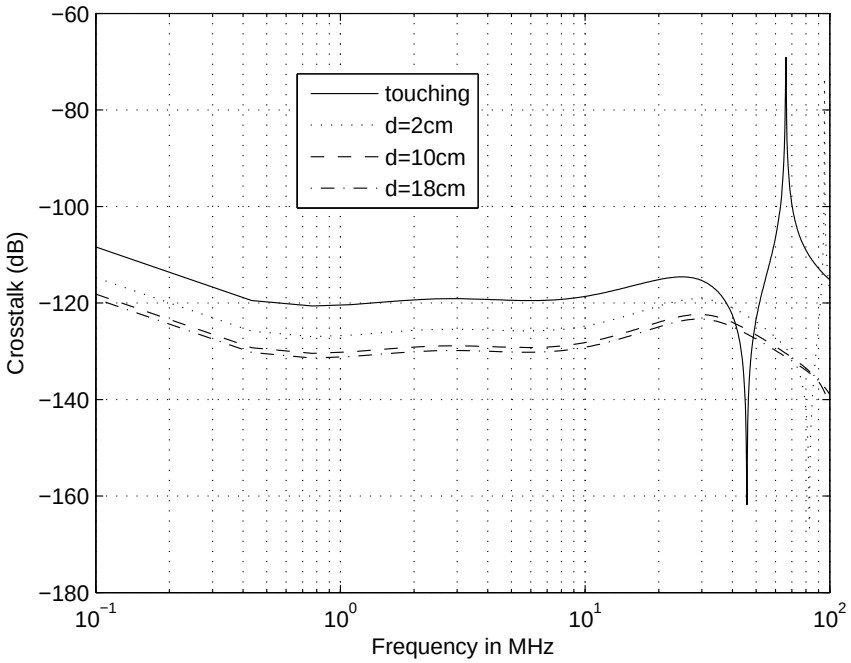

Figure 18: Simulation Crosstalk in two RG58 coax cables (l= 2m, and common connector plates)using a simple low frequency model and the Klay model of the transfer impedance.

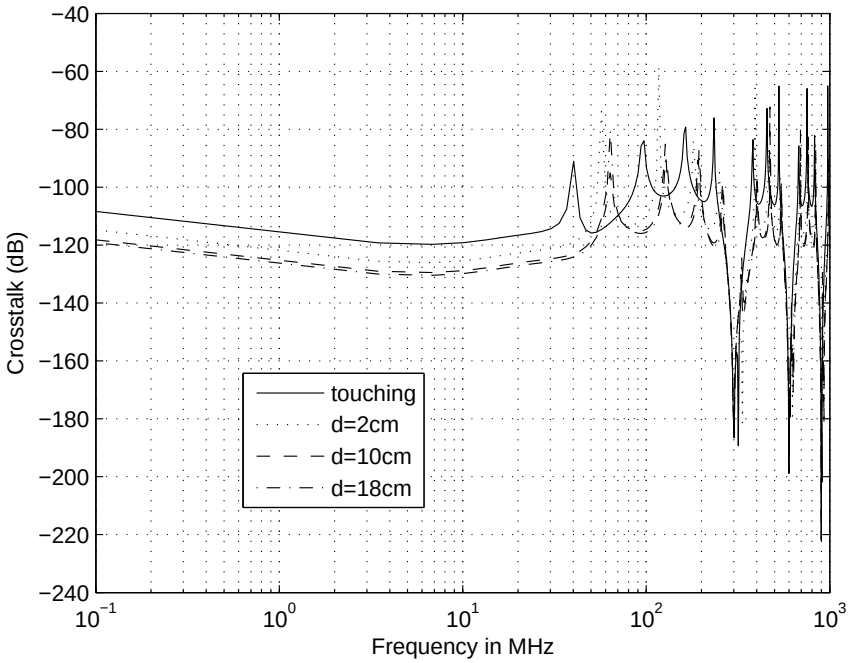

Figure 19: Simulation Crosstalk in two RG58 coax cables (l= 2m, and common connector plates)using a high frequency model and the Klay model [3] of the transfer impedance.

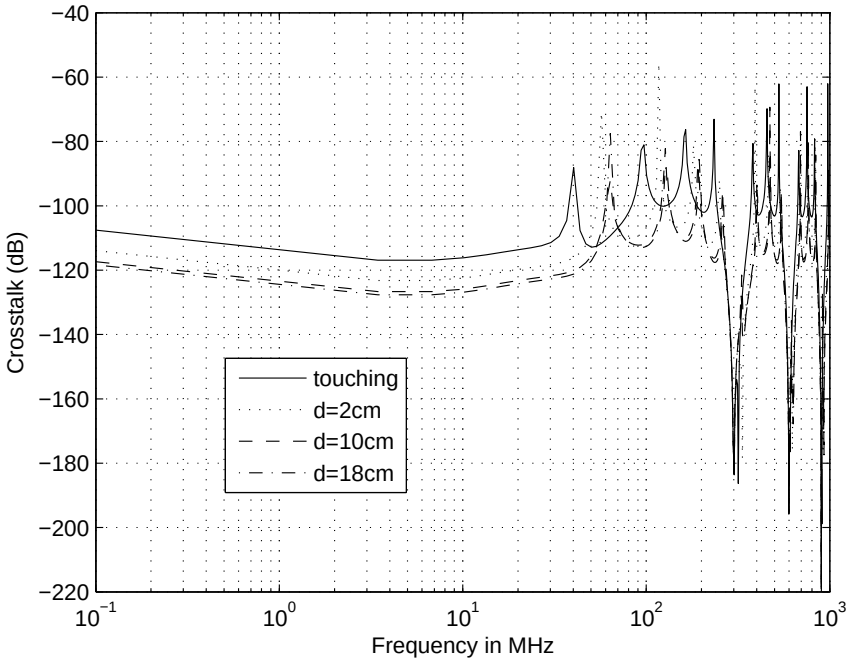

Figure 20: Simulation Crosstalk in two RG58 coax cables (l= 2m, and common connector plates)using a high frequency model and the Klay model [3] of the transfer impedance and the upper bound of the expected transfer impedance ($Z_t + \sigma_{Zt}$) given manufacturing tolerances.

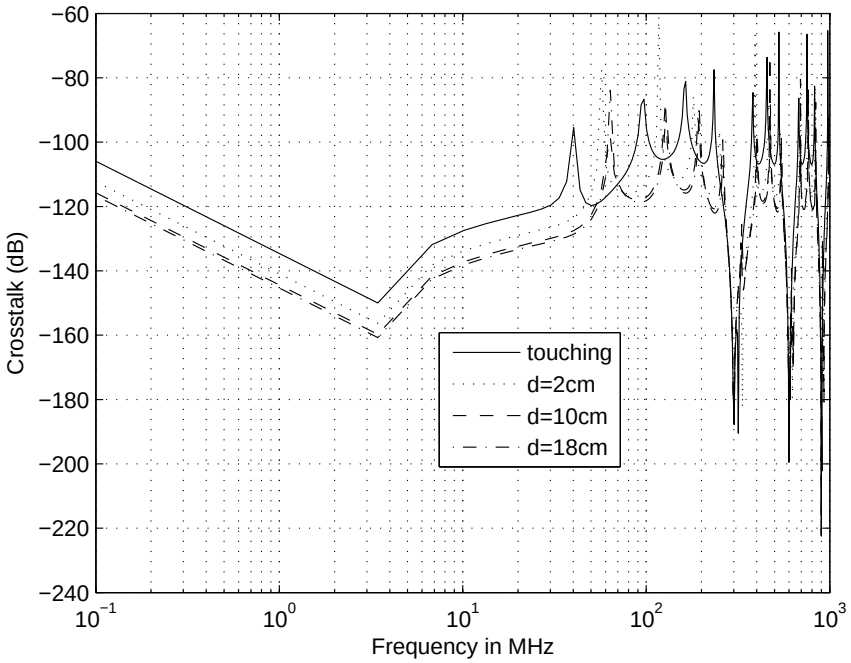

Figure 21: Simulation Crosstalk in two RG58 coax cables (l= 2m, and common connector plates)using a high frequency model and the Vance model [1] of the transfer impedance

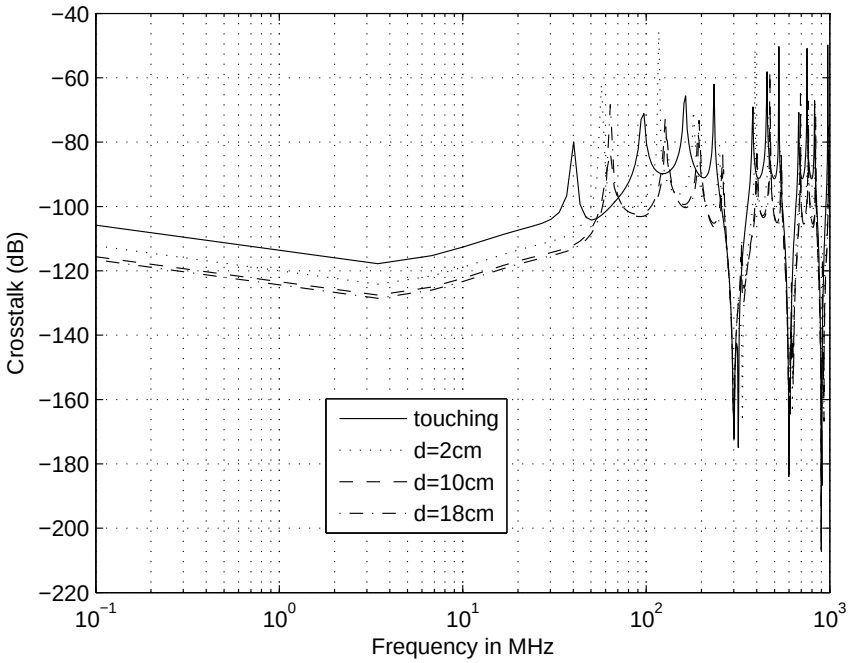

Figure 22: Simulation Crosstalk in two RG58 coax cables (l= 2m, and common connector plates)using a high frequency model and the Tyni model [2]of the transfer impedance

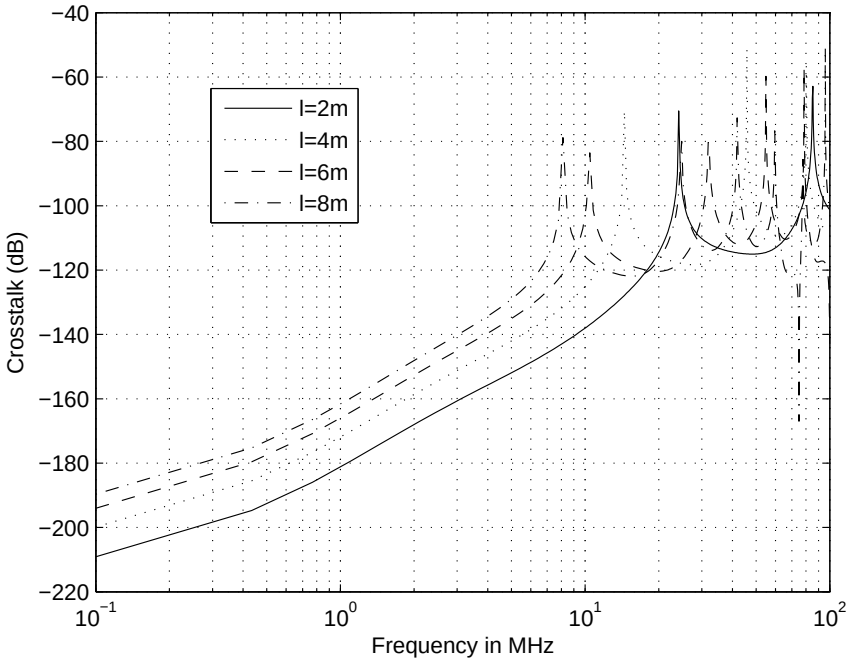

Figure 23: Simulation Crosstalk in two RG58 coax cables (d= 5cm, and **no** common connector plate at remote termination)using a high frequency model and the Kley model [3]of the transfer impedance

parameters that can only be roughly estimated. How to address this to provide some useable results for practical engineers needs to be tackled in the future work.

The Klay [3] model of the braid transfer impedance appears to be sufficiently accurate as it is assumed the observed 10 dB underestimate of the cable coupling can be attributed to uncertainties in the braid parameters.

Up until the first resonance the cable coupling is normally very low ($< 100dB$). The frequency at which the first resonance occurs is normally less than the ideal half wavelength frequency due to stray reactances. The resonances were faithfully reproduced in the simulations by adding small inductances or capacitances at the terminations of the tertiary circuit (circuit comprising the cable braids and connector plates). The coupling model developed so far assumes the tertiary circuit is completely lossless so the maximum predicted coupling could be infinite. The only reason large peaks do not appear in the presented results in that the modelled tertiary circuit has a very high Q and frequency steps have not fallen exactly on the resonant points. For example Figure 24 shows the detail of a resonance point indicating a maximum coupling of 200 dB. A means of estimating the losses in the tertiary circuit is therefore required.

From these observations the proposed work plan for the next two months are;

- Complete coupling model to include the ground plane
- Find a practical way of estimating the stray reactances in the tertiary circuit and their uncertainty.
- Find a practical way of estimating the losses in the tertiary circuit and their uncertainty.
- Include the losses in the model of cable coupling
- Provide a practical estimate of cable coupling given the uncertainties in the parameters
- If there is time I will also look at multiple cable coupling

Appendix

cable parameters

Cable type	N	n	D_0 /mm	d /mm	l /mm	α
RG58	12	9	2.95	0.127	19.79	27.42
RG58-A	16	7	2.95	0.127	19.72	27.56
RG58-Rep	18	6	2.95	0.127	19.79	27.56

The RG58 and RG58-A parameters are from [5] and the RG58-Rep N and n parameters were provided by [7] with the rest taken from RG58-A

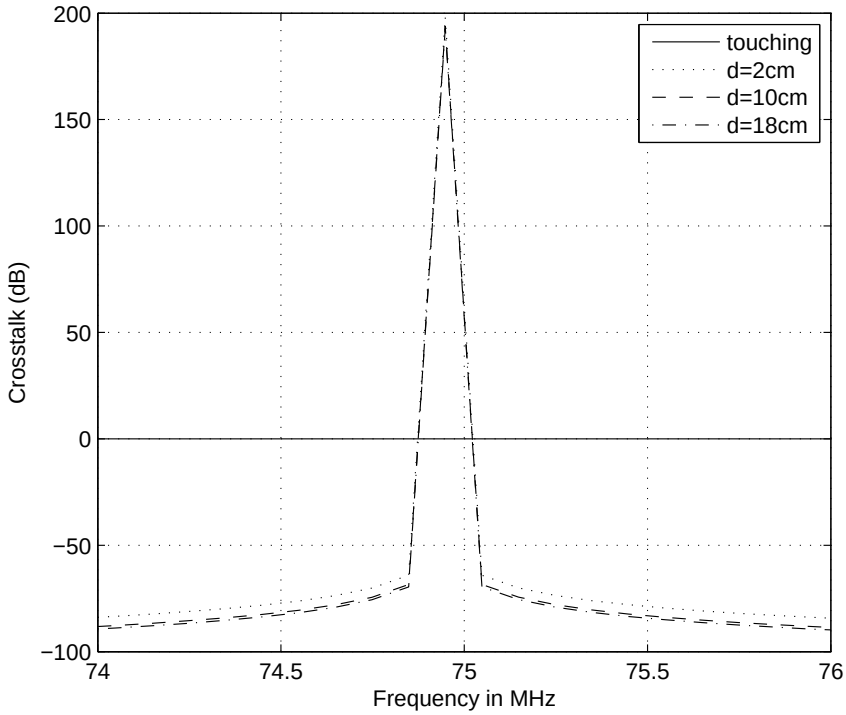

Figure 24: Detail os a simulated cable coupling resonance point for an ideal tertiary circuit of length 2m

comparison of nomenclature

This Report	Kley [3]	Vance [1]	Report [7]
P	-	P	-
N	m	$\mathcal{C}$	ζ
n	n	N	N
d	d	d	d
α	α	α	ψ
D_m	D_m	$2a$	$2b$
χ	B	K	χ
F	G	F	F
k_1	k_1	-	k
k_2	k_2	-	k
D_l	D_L	-	D_l
D_g	D_G	-	D_g

References

[1] E.F. Vance , *Shielding Effectiveness of braided-wire shields*, IEEE Trans. EMC, Vol 17, No. 2, 1975, pp 71-77.

[2] M. Tyni , *The transfer impedance of coaxial cables with braided conductors*, Proceedings of EMC symposium, Wroclow, Poland, Sept. 1976, pp 22-24.

[3] T. Kley , *Optimized single-braided cable shields*, IEEE Trans. EMC, Vol. 35, No. 1, 1993, pp 1-9.

[4] J.N. Katakis , *Transfer impedance of wire braided coaxial cables at radio and microwave frequencies*, MEng thesis, University of Sheffield, Feb. 1983.

[5] E.F. Vance , *Coupling to shileded cables*, 1978, Pub. A Wiley, ISBN 0-471-04107-6

[6] D.R.J. White and M Mardiguian, *A handbook series on EMI and Compatibility, Volume 3: Electromagnetic shielding*, 1988, Pub. Don White Consultants Inc., ISBN-13:978-0944916031

[7] J-C. Aldon, S. Antipolis and F. Leferink, *Transfer impedance of cables*, report 3.3 RCTR study 1997.

[8] F.A. Benson, P.A. Cudd and J.M. Tealby, *Leakage from coaxial cables*, IEE Proc-A, Vol. 139, No. 6, 1992, pp 285-303.

[9] S. Sali *Response of externally excited coaxial cables with wire braided shields*, IEE Proc. Sci. Meas. Technol., Vol 141, No. 4, 1994, pp 266-272

[10] S. Sali *A Circuit based approach for crosstalk between coaxial cables with optimum braided shields*, IEEE Trans. EMC, Vol 35, No. 2, 1993, pp 300-311.

[11] L. Korteweg *Crosstalk in cables*, Internship report, Thales Nederlands B.V., January 2008.